2025, 65(10): 4374-4391
CSTR: 32112.14.j.AMS.20240834
DOI: 10.13343/j.cnki.wsxb.20240834

微生物学报
Acta Microbiologica Sinica
http://journals.im.ac.cn/actamicrocn

Research Article 研究报告

基于基因组尺度代谢网络模型的大肠杆菌遗传修饰用于积累丙酮酸

李雪菲，郭超豪，同雯玥，杨森，刘晓云，李景晨*，康明*

河北大学 生命科学学院，河北 保定

李雪菲, 郭超豪, 同雯玥, 杨森, 刘晓云, 李景晨, 康明. 基于基因组尺度代谢网络模型的大肠杆菌遗传修饰用于积累丙酮酸[J]. 微生物学报, 2025, 65(10): 4374-4391.

LI Xuefei, GUO Chaohao, TONG Wenyue, YANG Sen, LIU Xiaoyun, LI Jingchen, KANG Ming. Genome-scale metabolic network model-guided genetic modification of *Escherichia coli* for pyruvate accumulation[J]. Acta Microbiologica Sinica, 2025, 65(10): 4374-4391.

摘　要：【目的】利用基因组尺度代谢网络模型指导大肠杆菌的遗传修饰，构建可积累丙酮酸的突变株。【方法】以基因组规模的代谢网络模型为指导，模拟大肠杆菌丙酮酸的积累过程，筛选代谢途径中的关键基因，并确定基因编辑策略。具体敲除乙酸激酶基因 *ackA*、磷酸乙酰转移酶基因 *pta*、乙醇脱氢酶基因 *adhE*、糖原合成酶基因 *glgA*、糖原磷酸化酶基因 *glgP*、磷酸戊糖焦磷酸(PRPP)合酶基因 *prs*、核糖 1,5-二磷酸磷酸激酶基因 *phnN* 和转运蛋白编码基因 *proP*；敲入转运蛋白编码基因 *ompC*、类黄酮毒素基因 *fldA* 和 D-丝氨酸氨裂解酶基因 *dsdA*。【结果】基因编辑突变株 MG1655-6-2 在厌氧条件下进行摇瓶发酵，丙酮酸产量达 10.46 g/L，转化率为 0.69 g/g。代谢组分析表明，发酵液中丙酮酸水平显著升高，某些相关代谢副产物显著降低。通过 5 L 补料分批发酵和适应性实验室进化，该菌株的最终丙酮酸产量达到 45.86 g/L。【结论】本研究证实了一种基因编辑策略的有效性，即基于基因组规模的代谢网络模型预测的基因编辑策略，可在厌氧条件下提高大肠杆菌丙酮酸产量，为微生物代谢工程提供了有价值的参考。

关键词：大肠杆菌；丙酮酸；基因组规模的代谢网络模型；CRISPR-Cas9；适应性实验室进化

资助项目：河北省重点研发计划(21372803D)
This work was supported by the Hebei Provincial Key Research and Development Project (21372803D).
*Corresponding authors. E-mail: KANG Ming, mingkang@hbu.edu.cn; LI Jingchen, lijingchen@hbu.edu.cn
Received: 2024-12-22; Accepted: 2025-07-13; Published online: 2025-08-18

Genome-scale metabolic network model-guided genetic modification of *Escherichia coli* for pyruvate accumulation

LI Xuefei, GUO Chaohao, TONG Wenyue, YANG Sen, LIU Xiaoyun, LI Jingchen*, KANG Ming*

College of Life Sciences, Hebei University, Baoding, Hebei, China

Abstract: [Objective] To construct an *Escherichia coli* mutant strain that accumulates pyruvate by genetic modification guided by the genome-scale metabolic network model. **[Methods]** Using a genome-scale metabolic network model as a guide, we simulated pyruvate production of *E. coli*, screened key genes in metabolic pathways, and developed gene editing procedures accordingly. We knocked out the acetate kinase gene *ackA*, phosphate acetyltransferase gene *pta*, alcohol dehydrogenase *adhE*, glycogen synthase gene *glgA*, glycogen phosphorylase gene *glgP*, phosphoribosyl pyrophosphate (PRPP) synthase gene *prs*, ribose 1,5-bisphosphate phosphokinase gene *phnN*, and transporter encoding gene *proP*. Furthermore, we knocked in the transporter encoding gene *ompC*, flavonoid toxin gene *fldA*, and D-serine ammonia lyase gene *dsdA*. **[Results]** A shake flask process with the genetically edited mutant strain MG1655-6-2 under anaerobic conditions produced pyruvate at a titer of 10.46 g/L and a yield of 0.69 g/g. Metabolomic analysis revealed a significant increase in the pyruvate level in the fermentation broth, accompanied by notable decreases in the levels of certain related metabolic byproducts. Through 5 L fed-batch fermentation and an adaptive laboratory evolution, the strain finally achieved a pyruvate titer of 45.86 g/L. **[Conclusion]** This study illustrated the efficacy of a gene editing strategy predicted by a genome-scale metabolic network model in enhancing pyruvate accumulation in *E. coli* under anaerobic conditions and provided novel insights for microbial metabolic engineering.

Keywords: *Escherichia coli*; pyruvate; genome-scale metabolic network model; CRISPR-Cas9; adaptive laboratory evolution

Pyruvate, a tri-carbon ketoacid derived from glucose catabolism in living organisms, serves as a crucial intermediate molecule for cellular metabolisms. Generated *via* the glycolytic pathway, pyruvate subsequently enters the tricarboxylic acid cycle upon oxidation, fuels many metabolic pathways and reactions and plays a pivotal role in bioenergy metabolism. Pyruvate also acts as a precursor for the synthesis of various other chemicals and compounds, including 2,3-butanediol, ethylene polymers, and L-alanine, which find widespread applications in diverse industrial sectors[1]. The global market size for pyruvate was $ 44 million in 2020 and is projected to reach $ 61 million by 2027, with an annual growth rate of 4.5% during the forecast period, highlighting a strong demand for pyruvate, according to the market report by Business Research Insights (https://www.businessresearchinsights.com/zh/market-reports/pyruvic-acid-market-109174).

Escherichia coli has become the most widely used chassis organism for synthesizing various target products, due to its well elucidated genetic background and capacity of high cell-density

fermentation. The advent of metabolic engineering and synthetic biology has facilitated the development of multiple methods to enhance pyruvate production. Primarily produced through glycolysis, pyruvate serves as its end product, and its yield is influenced by glycolytic flux. Because of the stringent regulation of carbon metabolism in *E. coli*, overexpressing pyruvate kinase (PYK) and phosphofructokinase (PFK) does not substantially elevate glycolytic flux[2]. Instead, the flux can be modulated by global cofactors, such as NADH and ATP, within cells[3]. Elevated NADH levels inhibit the enzymatic activity of pyruvate dehydrogenase complex (PDHc). Thus, altering the NADH/NAD^+ ratio through cofactor engineering can augment pyruvate production[4]. Additionally, modifying the *atp* operon enables *E. coli* to decouple respiration and increase glycolytic flux[5].

Furthermore, these modifications generally diminish the production of other metabolites derived from pyruvate catabolism. Pyruvate primarily degrades into acetyl-CoA and enters the TCA cycle catalyzed by PDHc aerobically, whereas under anaerobic conditions, it forms mixed acids controlled by pyruvate formate-lyase (PFL) [6]. Typically, genetic engineering techniques are employed to knock out or mutate specific genes, introduce alternative genes, and adjust promoter strength, thereby directing more carbon sources towards target molecule(s) production. For instance, site-directed mutagenesis of the PDH-encoding gene (*aceE*), and knockout of genes encoding PFL (*pflB*), alcohol dehydrogenase (*adhE*), pyruvate oxidase (*poxB*), acetate kinase (*ackA*), and lactate dehydrogenase (*ldhA*), are strategies to obstruct byproduct synthesis pathways[7-9].

However, the common genetic modification means based on metabolic pathway analysis have certain limitations. Because they mainly rely on the collections of the individual, separated, scattered metabolic study data to decide the engineering targets, lacking enough information related the correlation and coordination of metabolic networks, thus resulting in low efficiency or backward in genetic manipulation processes[10]. More comprehensive and efficient methods are needed to give guidance for the correlation exploration and overall coordination of various targeted genetic manipulation. The genome-scale metabolic network model (GEM) is an important tool for assessing the effects of genetic interventions and environmental perturbations on cellular metabolism[11]. It systematically characterizes microorganisms using computer language, based on gene-protein-reaction (GPR) relationships and energy balances within microbial metabolic pathways[12]. The feasibility of studying biological metabolism through GEM was established in 1999 with the construction of the first GEM, iJE330[13]. Currently, GEMs for over 150 microorganisms, including *E. coli*, *Corynebacterium glutamicum*, and a few of filamentous fungi, have undergone continuous construction, optimization, and application[14-17]. Furthermore, GEM finds its applications in addressing a range of biological inquiries, such as metabolic engineering, model-driven discoveries, prediction of cell phenotypes, analysis of biological network characteristics, evolutionary process studies, and interspecies interactions[18]. Specifically, GEMs aid in simulating the overall metabolic reaction characteristics, metabolic pathway stability, and metabolite distribution.

With the development and enhancement of algorithm tools and biochemical databases,

numerous intelligent model construction platforms have been established and updated, firmly supporting the generation of high-quality GEMs. Flux balance analysis (FBA) stands as the most widely-used algorithm for predicting the overall relationships among the absorption rates of diverse nutrients, metabolite synthesis rates, and cell growth rates[19]. Additionally, it aids in identifying the genes related to target products[20-21]. Recently several researchers have employed various algorithms to forecast gene targets within succinate synthetic pathways for enhancing the yield of succinate in *E. coli*[22-24].

A model of *E. coli* K-12 MG1655 named iJO1366 was established in 2011, exploring 1 366 genes, 2 251 metabolic reactions and 1 136 unique metabolites[25]. iJO1366 was updated based on an earlier model iAF1260, and a total of 107 new genes were added and 1 gene removed compared to model iAF1260. It is the most state-of-the-art model and the most comprehensive metabolic reconstruction in any microorganism to date and can serve as a basis for metabolic reconstructions in other bacteria.

Given the progress of GEMs and importance of pyruvate production by fermentation, GEM technique has not been applied in the construction of *E. coli* pyruvate producers yet. In this study, we began with the *E. coli* K-12 MG1655 model, iJO1366, as our basic model, and incorporated the latest pyruvate metabolism data from databases to refine and stabilize it. We simulated the anabolic and catabolic processes of pyruvate in MG1655 wild-type (WT) strain, aiming to pinpoint genes beneficial for pyruvate production. Gene knockout, knock-in, and site-directed mutagenesis techniques utilizing CRISPR/Cas9 enhanced cellular glucose uptake and facilitated a higher conversion rate of carbon sources to pyruvate. These genetically altered strains underwent anaerobic fermentation in shake flasks for 22 hours. Consequently, one of the mutant strains, MG1655-6-2 (Δ*ackA-pta*Δ*adhE*Δ*glgAP*::*fldA*Δ*proP*::*ompC*), exhibited a titer of 10.46 g/L pyruvate and a yield of 0.69 g/g. We analyzed the untargeted metabolome of the mutant strain, and identified differential metabolites through multivariate statistical analysis. This allowed us to determine the metabolic shifts and volumetric changes before and after gene editing, confirming the improvement of pyruvate production capabilities in the manipulated strain. The titer of the mutant strain through fed-batch fermentation was 35.94 g/L and the yield was 0.70 g/g. Ultimately, we conducted adaptive laboratory evolution (ALE) in a 5 L fermentation tank, achieving a titer of 45.86 g/L. This study presented hopeful ideas for constructing *E. coli* strains capable of anaerobic fermentation for pyruvate production.

1 Materials and Methods

1.1 *In silico* analysis of pyruvate biosynthetic pathway and gene editing

The iJO1366 model was employed for the *in silico* simulation of *Escherichia coli* with the COBRA toolbox (v3.1) in MATLAB (R2020b)[26]. Pyruvate metabolism information was searched and collected from KEGG (https://www.kegg.jp/) and added to the iJO1366 model using the online tool CAVE (https://cave.biodesign.ac.cn/)[27].

The biosynthetic pathway of pyruvate was simulated using FBA in order to investigate its characteristics. Glucose was utilized as the sole carbon source, with an uptake rate set at 18.5 mmol/(g DW·h). The uptake rate of oxygen was

set at 0 mmol/(g DW·h) under anaerobic conditions.

Flux variability analysis (FVA) was derived from FBA, which predicts the optimal fluctuation range of various reactions under ideal conditions and obtains candidate reactions for gene editing[28]. OptKnock is an algorithm that utilizes a hybrid bilevel optimization framework and linear programming duality theory to identify the optimal metabolic pathway for biochemical overproduction[29]. OptGene, an evolutionary approach, extends the applicability of the OptKnock method by using the principle of Darwinian evolution to formalize the search for the global optimal solution[30]. On the basis of candidate reactions, OptGene along with OptKnock were used to screen for gene editing target reactions.

1.2 Strains and plasmids construction

Strains and plasmids used in this study are listed in Table 1. The *E. coli* K-12 MG1655 strain (ATCC 700926) [F-lambda-*ilv*G-*rfb*-50 *rph*-1] and DH5α (F-φ80*lac*ZΔM15Δ (*lac*ZYA-*arg*F) U169 *end*A1 *rec*A1 *hsd*R17 (rk−, mk+) *sup*E44λ-*thi*-1 *gyr*A96 *rel*A1 *pho*A) were used as wild-type (WT) strains for the construction of pyruvate producer and cloning of the pEcCas and pEcgRNA plasmids respectively[31]. Subsequently, the modified MG1655 variants were obtained through CRISPR/Cas9 technology. Primer sequence information was described in Table 2.

Table 1 Strains and plasmids used in this study

Strain or plasmid	Relevant characteristics	Source
Escherichia coli		
DH5α	(F-φ80*lac*ZΔM15Δ(*lac*ZYA-*arg*F) U169 *end*A1 *rec*A1 *hsd*R17 (rk−, mk+) *sup*E44λ-*thi*-1 *gyr*A96 *rel*A1 *pho*A)	Lab collection
MG1655 WT	MG1655 (ATCC 700926) [F-lambda-*ilv*G-*rfb*-50 *rph*-1]	Lab collection
MG1655-2	*ackA-pta*	This study
MG1655-3	*ackA-pta-adhE*	This study
MG1655-4	*ackA-pta-adhE-glgA*	This study
MG1655-5	*ackA-pta-adhE-glgAP*	This study
MG1655-6a	*ackA-pta-adhE-glgAP-phnN*	This study
MG1655-6	*ackA-pta-adhE-glgAP-proP*	This study
MG1655-6-1	*ackA-pta-adhE-glgAP-proP*::*ompC*	This study
MG1655-6-2	*ackA-pta-adhE-glgAP*::*fldA-proP*::*ompC*	This study
MG1655-6-3	*ackA-pta*::*dsdA-adhE-glgAP*::*fldA-proP*::*ompC*	This study
Plasmid		
pEcCas	*Cas9*, *exo*, *beta*, *gam*, *sacB*, pSC101	[31]
pEcgRNA	*pMB1*, *ori*, *smR*, *J23119*, *ccdB*	[31]
pEcgRNA-*ackA-pta*	*pMB1*, *aadA*, *sgRNA-ackA-pta*	This study
pEcgRNA-*adhE*	*pMB1*, *aadA*, *sgRNA-adhE*	This study
pEcgRNA-*glgA*	*pMB1*, *aadA*, *sgRNA-glgA*	This study
pEcgRNA-*prs*	*pMB1*, *aadA*, *sgRNA-prs*	This study
pEcgRNA-*phnN*	*pMB1*, *aadA*, *sgRNA-phnN*	This study
pEcgRNA-*proP*	*pMB1*, *aadA*, *sgRNA-proP*	This study
pEcgRNA-*fldA*	*pMB1*, *aadA*, *sgRNA-fldA*	This study
pEcgRNA-*dsdA*	*pMB1*, *aadA*, *sgRNA-dsdA*	This study

Table 2 Sequences of the primers used in this study

Primers name	Primer sequences (5′→3′)
ackAptaFrw	CCACCACAATCCCTGCATGGGT
ackAptaRev	CATGATGATGCCAACGGCTGTCC
ackAptaFrwT	ACGTATCAATTATAGGTATCTCGTCATCATCCGCAGC
ackAptaRevT	GCTGCGGATGATGACGAGATACCTATAATTGATACGT
ackAptaN20Frw	CGAACAGCTGGAAGACAACGGTTTTAGAGCTAGAAATAGC
ackAptaN20Rev	CGTTGTCTTCCAGCTGTTCGACTAGTATTATACCTAGGAC
adhEFrw	CGGTTAGCTCCGAAGCAAAAGCCG
adhERev	GCCGTGCCAGTCATCCTTCAGG
adhEFrwT	CGCACTCGCCGCTTAATCAGTAGCGCTGTC
adhERevT	GATTAAGCGGCGAGTGCGTTAAGTTCAGCGAC
adhEN20Frw	GGATCAGGTTGATGTCTGGGGTTTTAGAGCTAGAAATAGC
adhEN20Rev	CCCAGACATCAACCTGATCCACTAGTATTATACCTAGGAC
glgAFrw	GCGTGGGCGATGAATATGTAAACGG
glgARev	GTTGAAAAACCTGCTAACCCGCC
glgAFrwT	GCAGCACCGGCAGCGGGAACATCTCTGAAC
glgARevT	TCCCGCTGCCGGTGCTGCAGGAAGGTTTCC
glgAN20Frw	TCGTGATACCTTCGCCGGACACTAGTATTATACCTAGGAC
glgAN20Rev	GTCCGGCGAAGGTATCACGAGTTTTAGAGCTAGAAATAGC
glgAPRev	CACTCGCCCCGAGAAAAATAGC
glgAPFrwT	CCCGCTGCGAAGTGGAAGAACTGCGTCGTC
glgAPRevT	CTTCCACTTCGCAGCGGGAACATCTCTGAAC
prsFrw	CGTTTTCGCGAGGTTGATGCG
prsRev	CATCCGTGAGCGCATCATCTG
prsFrwT	GAACTAGCACGATCGACACTGGCGGTACGC
prsRevT	GTGTCGATCGTGCTAGTTCCGGGGTGGC
prsN20Frw	ACCTGTGAAACGTTCGCACGGTTTTAGAGCTAGAAATAGC
prsN20Rev	CGTGCGAACGTTTCACAGGTACTAGTATTATACCTAGGAC
phnNFrw	CTTCCGACTACTACCCCGCC
phnNRev	CATCAAGCAGCGCCAGATGG
phnNFrwT	GTCCGGCTCCGGGAAAGACGCCAGTG
phnNRevT	GCGGGCGTTAATTTCACTGGCGTCTTTCCC
phnNN20Frw	CCAACAGATTTTGCCCCGCGGTTTTAGAGCTAGAAATAGC
phnNN20Rev	CGCGGGGCAAAATCTGTTGGACTAGTATTATACCTAGGAC
proPFrw	GGGGCAATGCTCGAGGAAATC
proPRev	GAAAGCTGCTGACCACCAGC
proPFrwT	CCGGGGGCTGGGTAGTGGCGGTGGTTGG
proPRevT	GCCACTACCCAGCCCCCGGGAAAAAAAC
proPN20Frw	GCATTACTCCGAAGACCACGGTTTTAGAGCTAGAAATAGC
proPN20Rev	CGTGGTCTTCGGAGTAATGCACTAGTATTATACCTAGGAC
ompCFrwT1	GGGGGCTGCCGCAGGCCCTTTGTTCG
ompCRevT1	GGCCTGCGGCAGCCCCCGGGAAAAAAAC
ompCFrwT2	CTATTTCCCCCGGTAGTGGCGGTGGTTGG
ompCRevT2	GCCACTACCGGGGGAAATAGATGTACAAGCGC
fldAFrwT1	CGATAATGCGTAGCACAGTGTGCAGTCCTG
fldARevT1	CTGTGCTACGCATTATCGCTCCTGTTTATGCCC
fldAFrwT2	CAAGTGGCGAGCTGCATCAGGTGCTGAC
fldARevT2	GCAGCTCGCCACTTGAACACCGGGAC
fldAN20Frw	CTGCGAAGTGGAAGAACTGCACTAGTATTATACCTAGGAC
fldAN20Rev	GCAGTTCTTCCACTTCGCAGGTTTTAGAGCTAGAAATAGC
dsdARev	CGGGTTCATCCACGAACTGGC
dsdAFrwT1	CCTGCCCGCGGCGCTACGCTCAATGAAAC
dsdARevT1	GTAGCGCCGCGGGCAGGTGGAAACATTCGG
dsdAFrwT2	CCTTTCCCTTGCTTAACTGCGCTGCATCAATG
dsdARevT2	GTTAAGCAAGGGAAAGGATTGCGATGCTGCG
dsdAN20Frw	TGCGCTGCGGATATCTGAACGTTTTAGAGCTAGAAATAGC
dsdAN20Rev	GTTCAGATATCCGCAGCGCAACTAGTATTATACCTAGGAC

1.3 Chemicals and reagents

All chemicals used in this study were purchased from Sinopharm Chemical Reagent Co., Ltd. (Shanghai, China) except the following ones: glycerol was purchased from LABGO (Tianjin, China), agar from BioFroxx (Guangzhou, China), methanol and acetonitrile from Tianjin Kemiou Chemical Reagent Co., Ltd. (Tianjin, China).

The Plasmid Miniprep Kit, DNA Gel/PCR Purification Miniprep Kit and Bacterial gDNA Miniprep Kit were all purchased from BEIWO (Hangzhou, China). The reagents used for PCR were purchased from Vazyme (Nanjing, China). Primer synthesis and DNA sequencing services were provided by Sangon Biotech Co., Ltd. (Shanghai, China). Glucose Assay Kit used for glucose detection in culture media was purchased from Leagene (Beijing, China).

1.4 Culture media and conditions

E. coli cells used in this study were cultivated at 37 °C in LB medium, shaken at 200 r/min during liquid culture. Kanamycin (50 μg/mL), spectinomycin (50 μg/mL), L-arabinose (60 mmol/L), L-rhamnose (100 mmol/L), or sucrose (10 mg/mL) was added to the medium as required. Strains were frozen-stored using 80% (*W/W*) glycerol at −80 ° C.

Seed medium for fermentation contained 12 g/L yeast extract, 24 g/L tryptone, 2.31 g/L KH_2PO_4, 16.43 g/L $K_2HPO_4 \cdot 3H_2O$ and 5 g/L glycerol. Fermentation medium contained 50 g/L glucose, 5 g/L yeast extract, 2 g/L KH_2PO_4, 1.5 g/L $MgSO_4 \cdot 7H_2O$, 33 g/L $(NH_4)_2SO_4$, 1.5 g/L betaine and 2 mL/L trace element mix.

1.5 Shake flask and fed-batch fermentation

All of the shake flask fermentation processes were performed in baffled flasks containing 40 mL of seed medium at 37 °C and shaken at 200 r/min. After the OD_{600} of the bacterial culture reached 10−15, 40 mL fermentation medium was added in each flask, and agitated at 35 °C. The flask was sealed with a solid silicone stopper during anaerobic fermentation.

A batch fermentation process started from a 3 L fermentation medium with a 10% inoculum in a 5 L bioreactor (Kelun, Shanghai, China). The processes were controlled at 37 °C and 400 r/min. 40% NaOH was used to control pH at 6.9 and 30% concentrated foam eliminator was used to remove foam in the fermenter. Dissolved-oxygen level was maintained to 30%. After the OD_{600} of the bacterial culture reached 15−18, the fermentation converted to the anaerobic stage. The agitation was adjusted to 300 r/min, and 60% glucose solution was fed by a feeding pump.

1.6 Adaptive laboratory evolution

Adaptive laboratory evolution (ALE) was performed using a 5 L bioreactor continuously. The basic method and process were the same as fed batch fermentation. During the continuous culture process, the feeding pump was controlled according to the experimental design. To restore the growth rate of the strains, M9 medium in which only simple nutrients included was used to conduct fed batch fermentation. A certain amount of sodium gluconate was added as carbon source in the early stages of ALE to shorten the generation time and to increase the amount of gene mutation and accelerate the evolutionary process. After 48 h of continuous culture, samples were taken to measure OD_{600} and residual sugar. An appropriate amount of fermentation broth was inoculated into a pre-sterilized 3 L medium with an initial OD_{600} of 0.4 to start next round of ALE. Following the continuous culture schedule, a new batch of ALE

was carried out every 48 h. The pyruvate titer and yield were monitored by HPLC from every other batch to evaluate the effect of ALE. Samples were collected from the last batch of culture, diluted and spread on LB agar plates to screen fast-growing single colonies, and stored in −80 ℃ freezer for future use.

1.7 Metabolites analytical procedures

Bacterial culture broths were centrifuged for 5 minutes at 6 000 r/min, and the supernatants were subsequently filtered through a 0.22 μm nylon filter. To measure the concentration of pyruvate, we utilized the Prominence LC-20AT HPLC system (Shimadzu, Japan), equipped with a Inertsil NH_2 column (GL Sciences, Japan) and a UV-VIS detector. The mobile phase eluent contained 30 mmol KH_2PO_4 buffer and methanol at a ratio of 6:4 (*V/V*). Pyruvate detection was performed at the wavelength of 225 nm and a temperature of 30 °C. The concentration of pyruvate was determined using the external standard calibration, based on the peak area comparison between the sodium pyruvate standard and that in samples.

An appropriate amount of fermentation broth supernatant was diluted using PBS buffer. The glucose concentration in the culture medium was quantified using a kit based on the O-toluidine boric method and a microplate reader, Spark Cyto (Tecan, Switzerland), was used to detect the absorbance at 630 nm.

1.8 Metabolomic analysis

Metabolomic analysis was applied to characterize the extracellular metabolites of *E. coli* K-12 MG1655 and its recombinant strains. The liquid chromatography-mass spectrometry (LC-MS) detection of fermentation components was run by the Ultra-high performance liquid chromatography Nexera UHPLC LC-30A (Shimadzu, Japan) and a mass spectrometer TripleTOF 6600+ (SCIEX, USA) coupled with a chromatographic column ACQUITY Premier HSS T3 (Waters, USA). The mobile phases for LC consisted of 25 mmol/L ammonium acetate and 25 mmol/L aqueous ammonia (mobile phase A) and acetonitrile (mobile phase B). Detailed MS parameters can be found in National Microbiology Data Center (http://nmdc.cn), No. NMDCX0002149. The data generated from the LC-MS assay were processed by multivariate statistical analysis, and the significantly changed metabolites (SCM) were screened using orthogonal partial least squares discriminant analysis (OPLS-DA). The LC-MS and metabolite statistical analysis were performed by Sangon Biotech Co., Ltd.

2 Results and Discussions

2.1 Metabolic flux analysis and knockout targets prediction for pyruvate accumulation

We have updated the *E. coli* iJO1366 model and provided a comprehensive list of Gene-Protein-Reaction associations (GPRs) related to pyruvate metabolism (Table 3). Utilizing the COBRA toolbox, we conducted a series of basic analyses on this updated model. These analyses encompassed growth calculations, robustness assessments, predictions of essential genes, as well as evaluations of metabolite connectivity and reaction participation (NMDCX0002149). Thus, we have verified the stability of the model structure, ensuring that the relevant data can be accurately understood and applied in subsequent studies.

Using FBA, we compared the metabolic flux distribution when the maximum growth rate and

Table 3 GPRs added to the iJO1366 model

Reaction abbreviation	Equation	GPRs
PYK2	ntp[c]+pyr[c]->ndp[c]+pep[c]	(Pyka (b1854)) or (Pykf (b1676))
LCADP	h2o[c]+mthgxl[c]+nadp[c]->pyc[c]+nadph[c]+h[c]	AldA (b1415)
MDH4	mal-L[c]+fad[c]->oaa[c]+fadh2[c]	Mqo (b2210)
CAAT	aca[c]+coa[c]<=>accoa[c]+amp[c]	Acs (b4069)
ACAT	ac[c]+atp[c]<=>aca[c]+ppi[c]	Acs (b4069)
LACH	mthgxl[c]+h2o[c]->lac-D[c]	HchA (b1967)
ALCD2x2	etoh[c]+nadp[c]<=>acald[c]+h[c]+nadph[c]	(YahK (b0325)) or (Ahr (b4269))

maximum pyruvate exchanges, that include the influxes and effluxes of pyruvate, were reached in WT strains under anaerobic conditions (Figure 1A, 1B). Under anaerobic conditions, when cells meet the require of maximum growth, the metabolic fluxes derived from the breakdown of glucose mainly are distributed in pentose phosphate pathway (PPP) and glycolytic pathway, as well are also directed to acetic acid due to the regulation of the *ackA* and *pta*, or decomposed into ethanol under the influence of the *adhE*, thereby affecting the accumulation of pyruvate (Figure 1C, 1E). In order to increase pyruvate producing, PPP and the catabolism of pyruvate should be downregulated, and the metabolic fluxes should be generally redirected toward pyruvate biosynthesis (Figure 1D, 1F). The maximum pyruvate exchange of 38.876 9 mmol/(g DW·h) in the ideal anaerobic case was estimated by the updated model. Gene targets were predicted by model simulation, aiming to modify these genes to guide more carbon sources to pyruvate accumulating machinery. All of the reactions and metabolites involved in Figure 1 are referred to as ORTH JD[25].

To assess the variability of pyruvate production under the same constraint conditions, we identified 103 reactions with practical significance and potential for equivalent substitution using FVA (NMDCX0002149). Through the screening of these alternative reactions by OptGene and OptKnock, a total of eight reactions were selected, and the corresponding genes associated with these reactions were targeted for gene editing (Table 4).

GLCS1 and GLCP play crucial roles in regulating the synthesis and phosphorylation of glycogen. This regulation enhances the activity of gluconeogenesis and the tricarboxylic acid cycle, leading to increased cell growth. During gluconeogenesis, pyruvate is significantly consumed as a carbon source[32-33]. By knocking out the corresponding genes, *i.e.*, the glycogen synthase gene (*glgA*) and the glycogen phosphorylase gene (*glgP*), the flow of carbon to glycogen metabolism can be blocked. This, in turn, allows more carbon and energy to be redirected towards the pyruvate biosynthesis.

PRPPS and R15BPK are both key reactions involved in the synthesis of phosphoribosyl pyrophosphate (PRPP), an essential precursor for the cellular synthesis of purine and pyrimidine nucleotides, coenzyme NAD, histidine, and tryptophan. When PRPP synthase gene (*prs*) is absent, mutant Δ*prs* can synthesize PRPP *via* the phosphorylation-driven pathway, a process regulated by the ribose 1,5-bisphosphate phosphokinase gene (*phnN*) in *E. coli*[34]. We hypothesize that *prs* and *phnN* could inhibit the

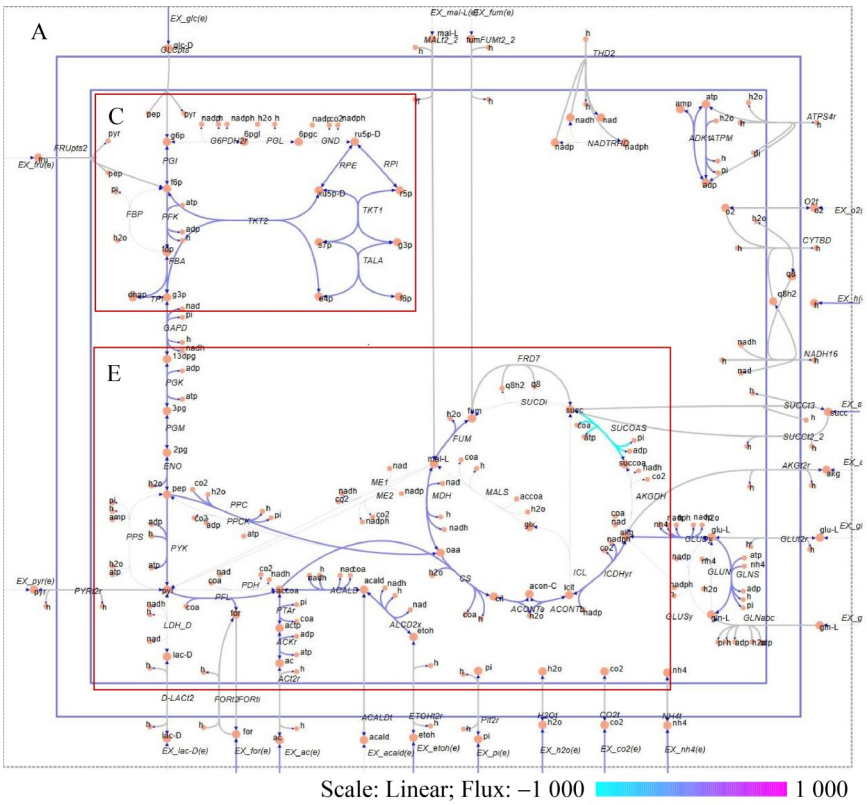
A
C
E
Scale: Linear; Flux: −1 000
1 000

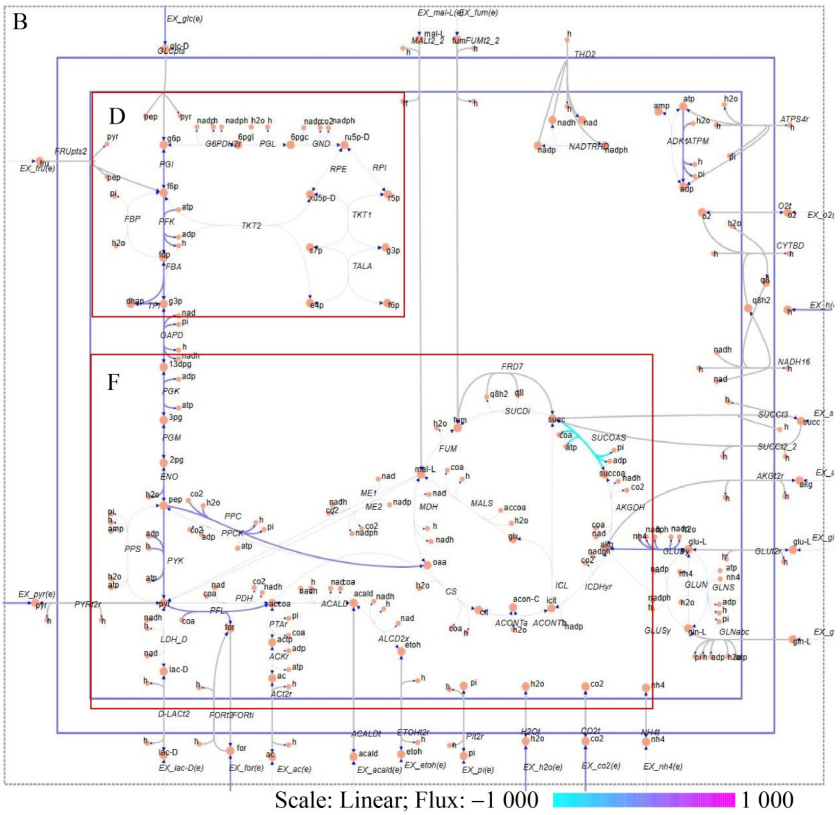
B
D
F
Scale: Linear; Flux: −1 000
1 000

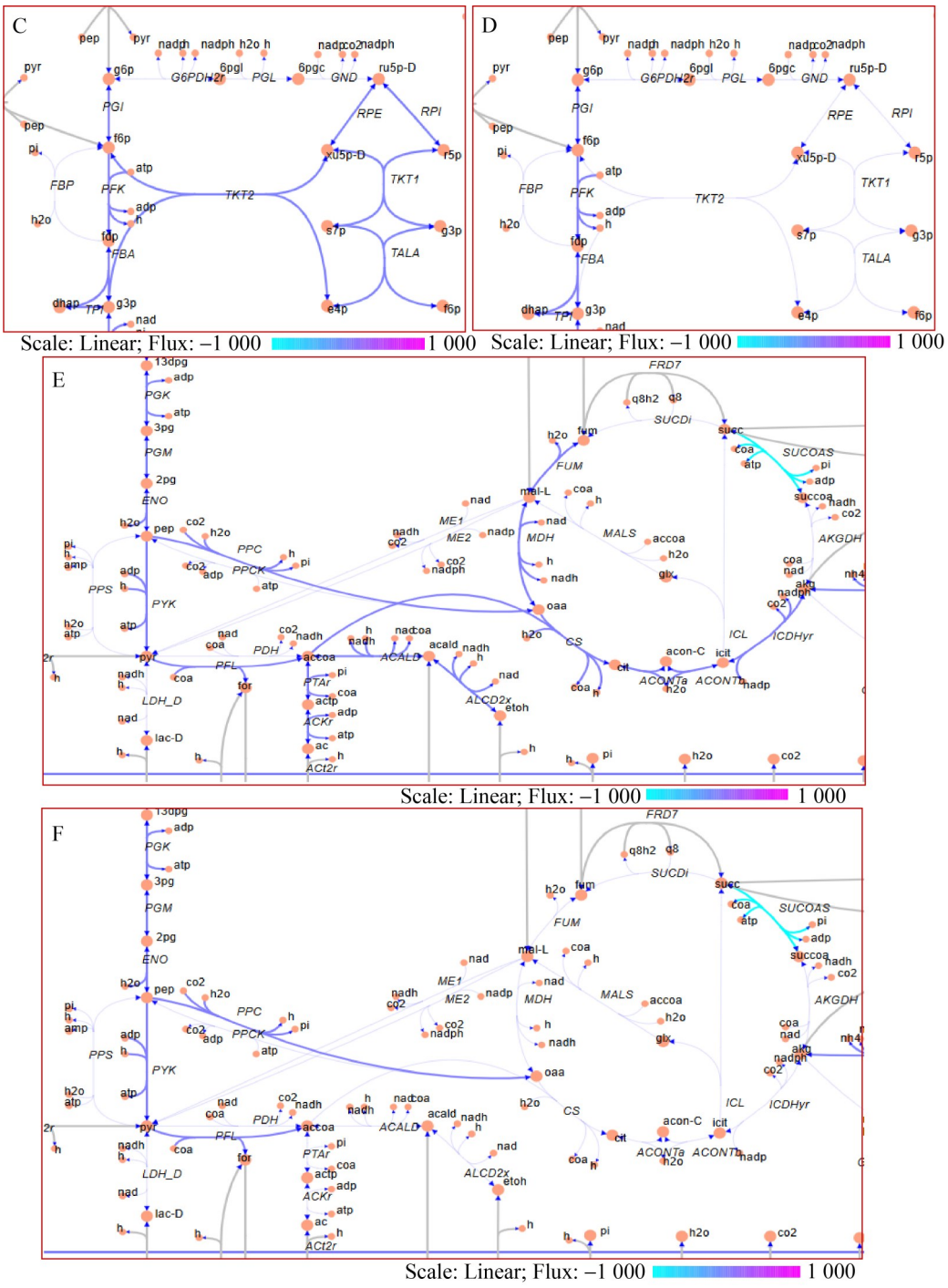

Figure 1 Flux distributions network maps under anaerobic conditions calculated by FBA. A: Flux distribution when cells reached maximal growth; B: Flux distribution when pyruvate effluxes and influxes reached the maximal level; C, D: The enlarged rectangle areas from A or B that show different flux distribution of PPP in the circumstances of A or B; E, F: The enlarged rectangle areas from A or B that reflect different flux distribution of pyruvate catabolism and TCA cycle in the circumstances of A or B. The reaction flux ranges are indicated by different colors from −1 000 mmol/(g DW·h) to 1 000 mmol/(g DW·h).

Table 4 Gene targets predicted by updated model

Gene	Reaction abbreviation	Equation
Knock out		
ackA	ACKr	ac[c]+atp[c]<=>actp[c]+adp[c]
pta	PTAr, PTA2	accoa[c]+pi[c]<=>actp[c]+coa[c] pi[c]+ppcoa[c]->coa[c]+ppap[c]
adhE	ACALD, ALCD2x	acald[c]+coa[c]+nad[c]<=>accoa[c]+h[c]+nadh[c] etoh[c]+nad[c]<=>acald[c]+h[c]+nadh[c]
glgA	GLCS1	adpglc[c]->adp[c]+glycogen[c]+h[c]
glgP	GLCP	glycogen[c]+pi[c]->g1p[c]
prs	PRPPS	atp[c]+r5p[c]<=>amp[c]+h[c]+prpp[c]
phnN	R15BPK	atp[c]+r15bp[c]->adp[c]+prpp[c]
proP	PROt2rpp	h[p]+pro-L[p]<=>h[c]+pro-L[c]
Knock in		
ompC	PYRtex	pyr[e]<=>pyr[p]
FldA	POR5, FLDR2	coa[c]+2 flxso[c]+pyr[c]<=>accoa[c]+co2[c]+2 flxr[c]+h[c] 2 flxso[c]+nadph[c]->2 flxr[c]+h[c]+nadp[c]
dsdA	SERD_D	ser-D[c]->nh4[c]+pyr[c]

synthesis of other molecules, such as histidine and tryptophan, resulting in decreased ATP consumption and increased pyruvate accumulation.

PROt2rpp and PYRtex are two independent reactions that express transporter proteins. The ProP protein transports zwitterionic osmolytes, such as glycine, betaine and proline, thereby mediating osmotic stress protection. Upon knocking out the *proP*, intracellular osmotic pressure was disrupted. However, this led to an increase in the absorption and utilization of carbon sources by cells[35]. When the ProP protein is inactive, OmpC and OmpF proteins can also transport betaine under low osmotic conditions, enhancing osmotic pressure tolerance in the later stages of fermentation[36]. This suggests that the aforementioned proteins might be involved in the uptake of glucose or other carbon sources, subsequently influencing the accumulation and efflux of pyruvate.

It is worth mentioning that, although the flavonoid toxin gene (*fldA*) and the D-serine ammonia-lyase gene (*dsdA*) have not been directly linked to pyruvate biosynthesis upon the existing knowledges, they are still involved in the accumulation of pyruvate[37].

2.2 Construction of pyruvate producing *E. coli* strains

The results of the genome scale metabolic network model provided us with unverified target genes for gene editing, which could guide a series of genetic manipulations to construct *E. coli* K-12 MG1655 mutants for pyruvate production. When the pEcgRNA-*prs* carrying a sgRNA to target *prs* and the linear fragment donor DNA for homologous recombination to generate mutant strain Δ*prs* were transformed into competent cells by electric shocks, no corresponding positive transformants were identified. In other words, strains with *prs* knocked out were unable to grow normally. This may be attributed to the reduced PRPP synthesis that is essential for cell growth.

The *phnN* has been reported to synthesize PRPP through an alternative pathway, the Δ*phnN* mutant could only survive when extra essential bases and amino acids were supplemented[34]. Therefore, nine gene-upregulated and down-regulated mutant strains were constructed by gene-edited strain modification except the failure of *prs* knockout and *phnN* kept intact also in partial of the mutant strains (Table 1).

2.3 Pyruvate production analysis

We used HPLC to detect the anaerobic fermentation broth of the modified strains from shake flasks for pyruvate accumulation, and calculated pyruvate titer using the external standard method (Figure 2). While disruption of *glgA* that prevent cells from utilizing pyruvate to generate glycogen performed, there was no significant difference in pyruvate production between the *glgA*-deletion mutant, MG1655-4, and the precedent strain MG1655-3. However, upon further knocking out *glgP*, the strain MG1655-5 was generated with a higher pyruvate accumulation. Subsequently, the pyruvate titer of the strain MG1655-6a declined compared to its predecessor, MG1655-5. We inferred that either the failure of *prs* knockout or the poor performance of Δ*phnN* resulted from being unable to synthesize PRPP normally or completely, which in turn prevented the redirection of more carbon sources towards pyruvate synthesis and potentially affected pyruvate accumulation through other unknown pathways. Therefore, the *phnN* was no longer knocked out in subsequent modified strains. Overall, most of the modified strains outperformed the WT strains in pyruvate production through shake flask fermentation, with

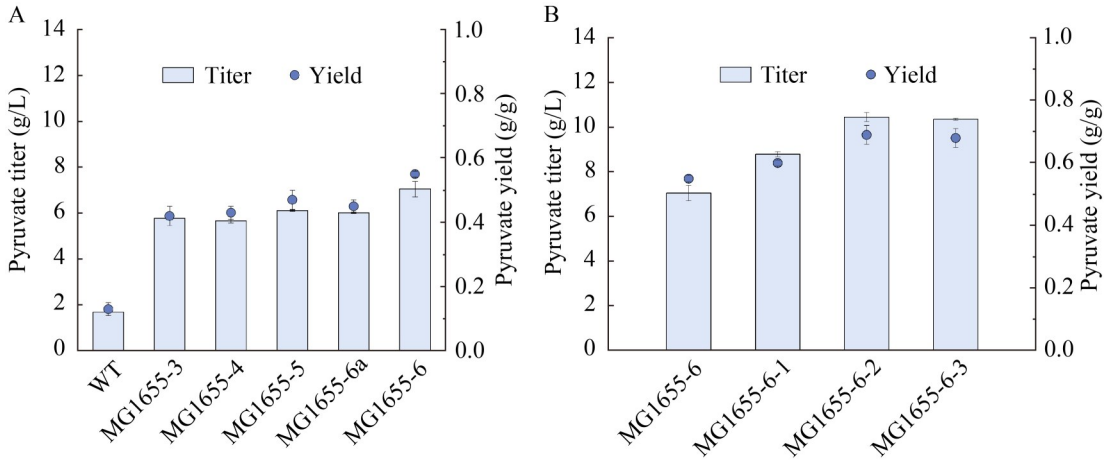

Figure 2 Pyruvate accumulation in genetically modified strains. A: The titer and yield of pyruvate from strains MG1655-3 (Δ*ackA*Δ*pta*Δ*adhE*), MG1655-4 (Δ*ackA*Δ*pta*Δ*adhE*Δ*glgA*), MG1655-5 (Δ*ackA*Δ*pta*Δ*adhE*Δ*glgAP*), MG1655-6a (Δ*ackA*Δ*pta*Δ*adhE*Δ*glgAP*Δ*phnN*), and MG1655-6 (Δ*ackA*Δ*pta*Δ*adhE*Δ*glgAP*Δ*proP*) that have genes knocked out; B: The titer and yield of pyruvate from strains MG1655-6-1 (Δ*ackA*Δ*pta*Δ*adhE*Δ*glgAP*Δ*proP*::*ompC*), MG1655-6-2 (Δ*ackA*Δ*pta*Δ*adhE*Δ*glgAP*::*fldA*Δ*proP*::*ompC*), and MG1655-6-3 (Δ*ackA*Δ*pta*::*dsdA*Δ*adhE*Δ*glgAP*::*fldA*Δ*proP*::*ompC*) that have genes knocked in. The titer and yield of strain MG1655-6 were included in Figure 2B for the convenient comparison among the strains with genes knocked out and knocked in. Columns indicate the pyruvate titer (g/L) achieved after 22 hours of anaerobic fermentation. Closed circles indicate the pyruvate yield (g/g). Error bars show standard deviations (*n*=3).

strain MG1655-6-2 achieving the highest titer, approximately six times higher than that of the WT strains. This might be due to the insertion of *ompC* and *fldA*, which improve the uptake and utilization of glucose by cells and allow more carbon to flow towards the synthesis of pyruvate. However, the knock-in of one more copy *dsdA*, which encodes D-seine dehydratase that mediates the deamination of D-serine into pyruvate when D-seine as sole carbon source[37], did not improve the accumulation of pyruvate at all, indicating that when glucose exists in the medium, the transcription of *dsdA* might be repressed or the activity of D-seine dehydratase be inhibited even though D-serine supplemented in the medium. But the hypothesis needs further solid experimental dada to support.

At the same time, we used the O-toluidine boric method to evaluate glucose consumption by the genetically modified strains and subsequently calculated the pyruvate yield (Figure 2). The glucose utilization of these strains gradually increased with the fermentation in progress, indicating that more carbons were being converted into pyruvate. Notably, the MG1655-6-2 strain exhibited the highest pyruvate yield, reaching 68.74%. This finding suggests that, in accordance with the model prediction results, knocking out or knocking in specific genes enhances the conversion of glucose to pyruvate, thereby leading to an increase in pyruvate production.

The shake flask broth of the WT strain and strain MG1655-6-2 were subjected to metabolome analysis. Multivariate statistical analyses, including principal component analysis and OPLS-DA, further confirmed that there are significant differences between the metabolite profiles of the two sample groups. A total of 175 SCMs were identified from strain MG1655-6-2, with 147 of them showing increased levels and 28 of them decreased when compared to the WT strain. Key SCMs between control and the experimental group are presented in Table 5. Among them, pyruvate exhibited a variable importance in projection (VIP) value of 1.46 and a significant increase in production. This analysis reveals that in strain MG1655-6-2 the pyruvate production was not only enhanced but also involved in the performance of other metabolic pathways.

A substantial alteration occurred in the strain's metabolic network following gene editing. Among these SCMs, pyruvate was significantly upregulated, while lactate was downregulated. Notably, the upregulated SCMs primarily clustered in pathways such as amino acid anabolism and co-factor metabolism. Citrate and malate exhibited considerable upregulation also, indicating an enhancement of the TCA cycle, that facilitates an overall elevation in the strain's metabolic level, leading to the production of numerous intermediate metabolites and ATP. Consequently, the carbon source is consumed more efficiently. The aforementioned results suggest that the metabolic networks of *E. coli* that experienced a series of gene editing still remain in a healthy state, thereby making it feasible to further upregulate the metabolic pathways that accumulate pyruvate and downregulate the metabolic pathways that consume pyruvate in order to enhance pyruvate production.

2.4 Adaptive laboratory evolution of strain MG1655-6-2

When strain MG1655-6-2 with optimal pyruvate production was cultured by a fed-batch fermentation, the pyruvate titer reached 35.94 g/L and the yield reached 0.70 g/g (Figure 3C). However, the growth of the strain exhibited a modest decline compared to that of the wild-type

Table 5 Key SCMs for experimental group (EG) *vs.* control check (CK)

SCM	Retention time (s)	VIP	*P*	Fold change	Trend
3-methyl-2-oxopentanoate	86.04	1.47	0.021 9	22.31	↑
Caryophyllene alpha-oxide	165.61	1.37	0.004 4	3.44	↑
Citraconic acid	176.02	1.37	0.002 3	7.21	↑
N,N-dimethylguanosine	123.17	1.48	0.002 3	10.54	↑
4-hydroxybenzaldehyde	183.70	1.36	0.012 0	6.39	↑
Adenosine	156.15	1.48	0.000 0	15.19	↑
Ellagic acid	226.06	1.51	0.001 2	0.08	↓
5′-methylthioadenosine	38.47	1.21	0.028 7	0.42	↓
Trimethylamine N-oxide	171.06	1.40	0.004 3	2.18	↑
4-yridoxic acid	71.85	1.43	0.011 6	0.59	↓
L-lactic acid	142.41	1.48	0.001 7	0.13	↓
Pyridoxine	44.27	1.40	0.021 1	29.09	↑
(-)-gallocatechin	116.09	1.17	0.000 3	17.48	↑
2-methoxy-3-(2-methylpropyl) pyrazine	89.08	1.54	0.006 7	614.81	↑
4-hydroxy-2-butenoic acid gamma-lactone	180.96	1.34	0.033 8	2.37	↑
Inosine	111.06	1.37	0.031 2	3.90	↑
2-(methylamino) benzoic acid	43.97	1.45	0.046 7	20.64	↑
Mannitol	182.76	1.41	0.007 3	9.91	↑
Pyrimidine	49.15	1.29	0.029 9	1.55	↑
6-acetyl-2,3-dihydro-2-(hydroxymethyl)-4(1H)-pyridinone	62.44	1.43	0.005 8	5.45	↑
lysoPE (16:0/0:0)	127.88	1.49	0.046 7	0.23	↓
2-benzofurancarboxaldehyde	183.47	1.39	0.000 9	6.83	↑
Acetylleucine	137.96	1.53	0.033 1	625.21	↑
Arecaidine	145.60	1.53	0.008 8	21.32	↑
2-aminoacrylic acid	227.90	1.33	0.016 5	165.94	↑
Protoanemonin	180.55	1.26	0.046 3	2.61	↑
Xi-3-hydroxy-5-phenylpentanoic acid O-beta-D-glucopyranoside	289.23	1.23	0.014 2	7.06	↑
3-aminocaproic acid	60.05	1.14	0.001 8	4.55	↑
Pyruvic acid	144.11	1.46	0.021 9	21.36	↑
L-beta-aspartyl-L-phenylalanine	236.94	1.19	0.021 3	3.44	↑
Isomaltose	127.36	1.34	0.019 3	0.11	↓
2-piperidinone	192.51	1.50	0.011 9	1.69	↑
Sepiapterin	91.46	1.51	0.035 9	0.07	↓
2-oxovaleric acid	197.16	1.35	0.034 3	2.54	↑
Choline	154.70	1.50	0.030 8	0.37	↓
L-pyroglutamic acid	252.33	1.47	0.000 5	3.63	↑
Beta-aminopropionitrile	2.53	1.36	0.019 9	1.49	↑
Porphobilinogen	180.13	1.16	0.049 2	1.88	↑
Trinexapac-ethyl	24.32	1.22	0.001 6	6.63	↑
Morpholine	70.52	1.01	0.021 1	5.37	↑
N-acetylserine	229.18	1.52	0.000 7	71.07	↑
Homocitrulline	226.90	1.35	0.036 1	5.28	↑
L-threonine	70.76	1.49	0.041 3	0.28	↓
2-phenylacetamide	183.88	1.36	0.001 0	6.63	↑
N′-formylkynurenine	200.76	1.17	0.000 4	18.62	↑
N-a-acetyl-L-arginine	219.97	1.10	0.002 1	6.55	↑
Beta-glycerophosphoric acid	251.57	1.44	0.000 1	9.34	↑
D-arginine	122.11	1.54	0.009 0	41.33	↑
Diphenylamine	198.85	1.51	0.042 7	17.50	↑
2,3-diethyl-5-methylpyrazine	100.72	1.35	0.005 0	0.15	↓

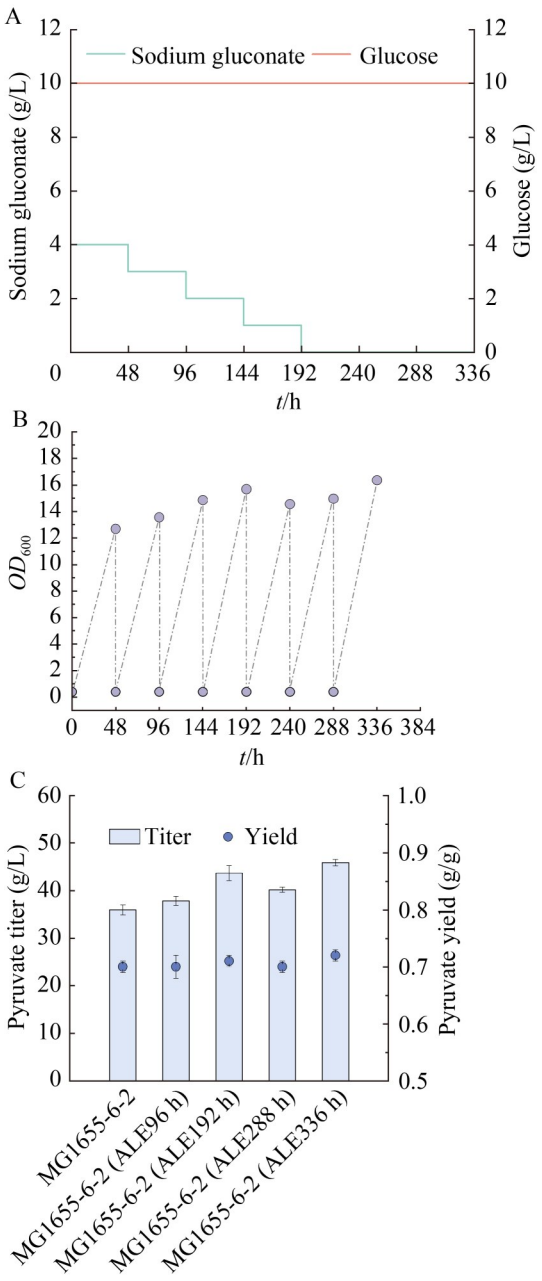

Figure 3 Adaptive laboratory evolution of strain MG1655-6-2. A: The supplements of sodium gluconate were gradually reduced from 4 g/L to 1 g/L in the first four batches (Green line indicates the supplements of sodium gluconate during the fermentation, and orange line indicates the glucose added); B: The changes of cell density during ALE (Closed circles indicate the absorbance at 600 nm (OD_{600})); C: Titers and yields of strain MG1655-2 monitored during ALE.

strain. Consequently, we performed an adaptive laboratory evolution (ALE) in a 5 L bioreactor, and MG1655-6-2 underwent continuous propagation over an extended period of time. We mimicked and expedited the natural evolutionary processes by conducting successive cultivations in a nutrient-limited medium with a progressively diminishing sodium gluconate supplements over the initial four batches (Figure 3A). To visualize the ALE course, we charted the cell density (OD_{600}) at the culmination of each batch on a linear graph (Figure 3B). Ultimately, we successfully screened an evolved strain MG1655-6-2 (ALE) with a pyruvate titer of 45.86 g/L and a yield of 0.72 g/g (Figure 3C).

3 Conclusion

Majority of the *E. coli* strains used in the industrial pyruvate fermentation processes were either modified by traditional random mutagenesis procedures or based on the metabolic pathway engineering strategies. These strains are commonly auxotrophic with complex fermentation processes and possess stability issues sometimes. In this study, we first used a GEM for simulating calculations and combined with metabolic pathway analysis to determine a novel modification strategy for creating *E. coli* pyruvate accumulating strains. It has been first ever reported in the construction of pyruvate producing microorganisms that the glycogen synthase gene *glgA*, the glycogen phosphorylase gene *glgP*, and the transporter encoding gene *proP* were knocked out, as well as the transporter encoding gene *ompC*, the flavonoid toxin gene *fldA*, and the D-serine ammonia lyase gene *dsdA* were knocked in, and the titers and yields of pyruvate were gradually improved except that of *dsdA*. The modified MG1655-6-2 strain can

stably produce pyruvate with less glucose consumption after ALE. In summary, our work provided a new idea and practice for using GEM to guide the construction of titer-and yield-improved pyruvate producing microorganisms.

Author contributions

LI Xuefei: Writing original draft, investigation, visualization, validation, data curation, and formal analysis; GUO Chaohao: Investigation, and visualization; TONG Wenyue: Investigation, and data analysis; YANG Sen: Investigation, and methodology; LIU Xiaoyun: Writing-review and editing, and supervision; LI Jingchen: Writing-review and editing, supervision, data analysis, funding acquisition, conceptualization, and project administration; KANG Ming: Writing-review and editing, supervision, resources, methodology, funding acquisition, conceptualization, and project administration.

Declaration of competing interest

The authors declare that they have no known competing financial interests or personal relationships that could have appeared to influence the work reported in this paper.

REFERENCES

[1] 刘立明, 李寅, 堵国成, 陈坚. 生物技术法生产丙酮酸的研究进展[J]. 生物工程学报, 2002, 18(6): 651-655.
LIU LM, LI Y, DU GC, CHEN J. Progress in biotechnological production of pyruvic acid[J]. Chinese Journal of Biotechnology, 2002, 18(6): 651-655 (in Chinese).

[2] OLIVER S. Demand management in cells[J]. Nature, 2002, 418(6893): 33-34.

[3] VEMURI GN, ALTMAN E, SANGURDEKAR DP, KHODURSKY AB, EITEMAN MA. Overflow metabolism in *Escherichia coli* during steady-state growth: transcriptional regulation and effect of the redox ratio[J]. Applied and Environmental Microbiology, 2006, 72(5): 3653-3661.

[4] LIU LM, LI Y, SHI ZP, DU GC, CHEN J. Enhancement of pyruvate productivity in *Torulopsis glabrata*: increase of NAD^+ availability[J]. Journal of Biotechnology, 2006, 126(2): 173-185.

[5] JENSEN PR, MICHELSEN O. Carbon and energy metabolism of *atp* mutants of *Escherichia coli*[J]. Journal of Bacteriology, 1992, 174(23): 7635-7641.

[6] KU JT, CHEN AY, LAN EI. Metabolic engineering design strategies for increasing acetyl-CoA flux[J]. Metabolites, 2020, 10(4): 166.

[7] CAUSEY TB, SHANMUGAM KT, YOMANO LP, INGRAM LO. Engineering *Escherichia coli* for efficient conversion of glucose to pyruvate[J]. Proceedings of the National Academy of Sciences of the United States of America, 2004, 101(8): 2235-2240.

[8] ZHU YH, EITEMAN MA, ALTMAN R, ALTMAN E. High glycolytic flux improves pyruvate production by a metabolically engineered *Escherichia coli* strain[J]. Applied and Environmental Microbiology, 2008, 74(21): 6649-6655.

[9] ZIEGLER M, HÄGELE L, GÄBELE T, TAKORS R. CRISPRi enables fast growth followed by stable aerobic pyruvate formation in *Escherichia coli* without auxotrophy[J]. Engineering in Life Sciences, 2022, 22(2): 70-84.

[10] SOMA Y, YAMAJI T, HANAI T. Dynamic metabolic engineering of *Escherichia coli* improves fermentation for the production of pyruvate and its derivatives[J]. Journal of Bioscience and Bioengineering, 2022, 133(1): 56-63.

[11] DAMIANI AL, HE QP, JEFFRIES TW, WANG J. Comprehensive evaluation of two genome-scale metabolic network models for *Scheffersomyces stipitis*[J]. Biotechnology and Bioengineering, 2015, 112(6): 1250-1262.

[12] ZHANG Y, CAI JY, SHANG XL, WANG B, LIU SW, CHAI X, TAN TW, ZHANG Y, WEN TY. A new genome-scale metabolic model of *Corynebacterium glutamicum* and its application[J]. Biotechnology for Biofuels, 2017, 10(1): 169.

[13] EDWARDS JS, PALSSON BO. Systems properties of the *Haemophilus influenzae* Rd metabolic genotype[J]. The Journal of Biological Chemistry, 1999, 274(25): 17410-17416.

[14] KIM B, KIM WJ, KIM DI, LEE SY. Applications of genome-scale metabolic network model in metabolic engineering[J]. Journal of Industrial Microbiology & Biotechnology, 2015, 42(3): 339-348.

[15] SHINFUKU Y, SORPITIPORN N, SONO M, FURUSAWA C, HIRASAWA T, SHIMIZU H. Development and experimental verification of a genome-scale metabolic model for *Corynebacterium glutamicum*[J]. Microbial Cell Factories, 2009, 8(1): 43.

[16] KIM TY, SOHN SB, KIM YB, KIM WJ, LEE SY. Recent advances in reconstruction and applications of genome-scale metabolic models[J]. Current Opinion Biotechnology, 2012, 23(4): 617-623.

[17] YE C, XU N, CHEN X, LIU L. Application of metabolic network model to analyze intracellular metabolism of

industrial microorganisms[J]. Chinese Journal of Biotechnology, 2019, 35(10): 1901-1913.
[18] McCLOSKEY D, PALSSON BØ, FEIST AM. Basic and applied uses of genome-scale metabolic network reconstructions of *Escherichia coli*[J]. Molecular Systems Biology, 2013, 9: 661.
[19] ORTH JD, THIELE I, PALSSON BØ. What is flux balance analysis[J]. Nature Biotechnology, 2010, 28(3): 245-248.
[20] VARMA A, PALSSON BO. Metabolic capabilities of *Escherichia coli* II. optimal growth patterns[J]. Journal of Theoretical Biology, 1993, 165(4): 503-522.
[21] LIU J, LIU MS, SHI T, SUN GN, GAO N, ZHAO XJ, GUO X, NI XM, YUAN QQ, FENG JH, LIU ZM, GUO YM, CHEN JZ, WANG Y, ZHENG P, SUN JB. CRISPR-assisted rational flux-tuning and arrayed CRISPRi screening of an L-proline exporter for L-proline hyperproduction[J]. Nature Communications, 2022, 13: 891.
[22] JIAN XX, LI NC, CHEN Q, HUA Q. Model-guided identification of novel gene amplification targets for improving succinate production in *Escherichia coli* NZN111[J]. Integrative Biology, 2017, 9(10): 830-835.
[23] MIENDA BS. *Escherichia coli* genome-scale metabolic gene knockout of lactate dehydrogenase (ldhA), increases succinate production from glycerol[J]. Journal of Biomolecular Structure and Dynamics, 2018, 36(14): 3680-3686.
[24] MIENDA BS, SHAMSIR MS, ILLIAS RM. Model-guided metabolic gene knockout of *gnd* for enhanced succinate production in *Escherichia coli* from glucose and glycerol substrates[J]. Computational Biology and Chemistry, 2016, 61: 130-137.
[25] ORTH JD, CONRAD TM, NA J, LERMAN JA, NAM H, FEIST AM, PALSSON BØ. A comprehensive genome-scale reconstruction of *Escherichia coli* metabolism: 2011[J]. Molecular Systems Biology, 2011, 7(1): 535.
[26] HEIRENDT L, ARRECKX S, PFAU T, MENDOZA SN, RICHELLE A, HEINKEN A, HARALDSDÓTTIR HS, WACHOWIAK J, KEATING SM, VLASOV V, MAGNUSDÓTTIR S, NG CY, PRECIAT G, ŽAGARE A, CHAN SHJ, AURICH MK, CLANCY CM, MODAMIO J, SAULS JT, NORONHA A, et al. Creation and analysis of biochemical constraint-based models using the COBRA toolbox v.3.0[J]. Nature Protocols, 2019, 14(3): 639-702.
[27] MAO ZT, YUAN QQ, LI HR, ZHANG Y, HUANG YY, YANG CH, WANG RY, YANG YF, WU YL, YANG SH, LIAO XP, MA HW. CAVE: a cloud-based platform for analysis and visualization of metabolic pathways[J]. Nucleic Acids Research, 2023, 51(W1): W70-W77.
[28] MAHADEVAN R, SCHILLING CH. The effects of alternate optimal solutions in constraint-based genome-scale metabolic models[J]. Metabolic Engineering, 2003, 5(4): 264-276.
[29] BURGARD AP, PHARKYA P, MARANAS CD. OptKnock: a bilevel programming framework for identifying gene knockout strategies for microbial strain optimization[J]. Biotechnology and Bioengineering, 2003, 84(6): 647-657.
[30] PATIL KR, ROCHA I, FÖRSTER J, NIELSEN J. Evolutionary programming as a platform for *in silico* metabolic engineering[J]. BMC Bioinformatics, 2005, 6(1): 308.
[31] LI Q, SUN B, CHEN J, ZHANG Y, JIANG Y, YANG S. A modified pCas/pTargetF system for CRISPR-Cas9-assisted genome editing in *Escherichia coli*[J]. Acta Biochim Biophys Sin (Shanghai), 2021, 53(5): 620-627.
[32] DEDHIA NN, HOTTIGER T, BAILEY JE. Overproduction of glycogen in *Escherichia coli* blocked in the acetate pathway improves cell growth[J]. Biotechnology and Bioengineering, 1994, 44(1): 132-139.
[33] ALONSO-CASAJÚS N, DAUVILLÉE D, VIALE AM, MUÑOZ FJ, BAROJA-FERNÁNDEZ E, MORÁN-ZORZANO MT, EYDALLIN G, BALL S, POZUETA-ROMERO J. Glycogen phosphorylase, the product of the *glgP* gene, catalyzes glycogen breakdown by removing glucose units from the nonreducing ends in *Escherichia coli*[J]. Journal of Bacteriology, 2006, 188(14): 5266-5272.
[34] HOVE-JENSEN B, ROSENKRANTZ TJ, HALDIMANN A, WANNER BL. *Escherichia coli* phnN, encoding ribose 1,5-bisphosphokinase activity (phosphoribosyl diphosphate forming): dual role in phosphonate degradation and NAD biosynthesis pathways[J]. Journal of Bacteriology, 2003, 185(9): 2793-2801.
[35] WANG SW, FANG Y, WANG Z, ZHANG SY, WANG LJ, GUO Y, WANG XY. Improving L-threonine production in *Escherichia coli* by elimination of transporters ProP and ProVWX[J]. Microbial Cell Factories, 2021, 20(1): 58.
[36] CATRON KM, SCHNAITMAN CA. Export of protein in *Escherichia coli*: a novel mutation in ompC affects expression of other major outer membrane proteins[J]. Journal of Bacteriology, 1987, 169(9): 4327-4334.
[37] LIM MY, LEE HJ, KIM P. Metagenome resource for D-serine utilization in a DsdA-disrupted *Escherichia coli*[J]. Journal of Microbiology and Biotechnology, 2011, 21(4): 374-378.